Microvascular Research 83 (2012) 337–346

Contents lists available at SciVerse ScienceDirect

Microvascular Research

journal homepage: www.elsevier.com/locate/ymvre

Quantification of the endothelial surface glycocalyx on rat and mouse blood vessels

Wan-Yi Yen, Bin Cai, Min Zeng, John M. Tarbell, Bingmei M. Fu *

Department of Biomedical Engineering, The City College of the City University of New York, 160 Convent Ave, New York, NY 10031, United States

ARTICLE INFO

Article history:
Accepted 3 February 2012
Available online 14 February 2012

ABSTRACT

The glycocalyx on the surface of endothelium lining blood vessel walls modulates vascular barrier function, cell adhesion and also serves as a mechano-sensor for blood flow. Reduction of glycocalyx has been reported in many diseases including atherosclerosis, inflammation, myocardial edema, and diabetes. The surface glycocalyx layer (SGL) is composed of proteoglycans and glycosaminoglycans, of which heparan sulfate is one of the most abundant. To quantify the SGL thickness on the microvessels of rat mesentery and mouse cremaster muscle *in situ*, we applied a single vessel cannulation and perfusion technique to directly inject FITC-anti-heparan sulfate into a group of microvessels for immuno-labeling the SGL. We also used anti-heparan sulfate for immuno-labeling the SGL on rat and mouse aortas *ex vivo*. High resolution confocal microscopy revealed that the thickness of the SGL on rat mesenteric capillaries and post-capillary venules is 0.9 ± 0.1 μm and 1.2 ± 0.3 μm, respectively; while the thickness of the SGL on mouse cremaster muscle capillaries and post-capillary venules is 1.5 ± 0.1 μm and 1.5 ± 0.2 μm, respectively. Surprisingly, there was no detectable SGL in either rat mesenteric or mouse cremaster muscle arterioles. The SGL thickness is 2.5 ± 0.1 μm and 2.1 ± 0.2 μm respectively, on rat and mouse aorta. In addition, we observed that the SGL is continuously and evenly distributed on the aorta wall but not on the microvessel wall.

Introduction

The luminal surfaces of endothelial cells (ECs) that line our vasculature are coated with a glycocalyx of membrane-bound macromolecules comprised of sulfated proteoglycans, hyaluronic acid, sialic acids, glycocproteins and plasma proteins that adhere to this surface matrix (Reitsma et al., 2007; Tarbell and Pahakis, 2006). This endothelial surface glycocalyx layer (SGL) plays an important role in regulating vascular permeability, attenuating interactions between circulating blood cells and the ECs, as well as sensing the hydrodynamic changes in the blood flow (Constantinescu et al., 2003; Curry and Adamson, 2010; Curry and Noll, 2010; Mulivor and Lipowsky, 2009; Pries et al., 2000; Reitsma et al., 2007; Tarbell, 2010; Wu et al., 2004). Damage to and modification of the endothelial SGL were found in many diseases such as diabetes, ischemia, myocardial edema, chronic infectious diseases and atherosclerosis (Becker et al., 2010; Chappell et al., 2011; Reitsma et al., 2007; van den Berg et al., 2003; VanTeeffelen et al., 2010; Weinbaum et al., 2007). Due to its crucial role in maintaining vascular functions, the structure and composition of the endothelial SGL has been widely studied since the 1960s (Adamson and Clough, 1992; Haldenby et al., 1994; Luft, 1966; Oohira et al., 1983; Squire et al., 2001; Vink and Duling, 1996).

The first visualization of the SGL by electron microscopy (EM) used the cationic dye ruthenium red that binds to acidic mucopolysaccharides and generates electron density in the presence of osmium tetroxide (Luft, 1966). Subsequent studies by Baldwin and Winlove (1984) and Clough and Moffitt (1992) used gold colloids and immunoperoxidase labeling (Baldwin and Winlove, 1984; Clough and Moffitt, 1992). Adamson and Clough (1992) then demonstrated using a large charged marker protein (unable to penetrate the SGL), cationized ferritin, that in the absence of plasma proteins, the SGL would collapse, presumably due to elimination of intramolecular interactions with plasma proteins, and that its undisturbed thickness was several times greater than the 20 nm observed with ruthenium red (Adamson and Clough, 1992; Luft, 1966). All of these methods may suffer from dehydration artifacts associated with aqueous fixatives that likely dissolve all but the protein cores of proteoglycans and collapse the inherently hydrated structures. A method developed to preserve water soluble structures using fluorocarbons as non-aqueous carriers of osmium tertroxide was applied to microvessels to obviate some of these limitations by Sims and Horne (Sims and Horne, 1993). Further elaborations of the fluorocarbon-glutaraldehyde fixation methods by Rostgaard and Qvortrup (1997) revealed a filamentous brush-like surface coating on capillary walls, but a layer thickness of <50 nm, suggesting a cleavage of more superficial matrix structures (Rostgaard and Qvortrup, 1997). All of the foregoing EM studies revealed an SGL with a thickness less than 100 nm. Recently, van den Berg et al. (2003) used a new approach to stabilize the anionic carbohydrate structures on the SGL by Alcian

* Corresponding author. Fax: +1 212 650 6727.
E-mail address: fu@ccny.cuny.edu (B.M. Fu).

0026-2862/$ – see front matter © 2012 Elsevier Inc. All rights reserved.
doi:10.1016/j.mvr.2012.02.005

blue 8GX (van den Berg et al., 2003). They found that the SGL thickness was 0.2–0.5 μm on rat left ventricular myocardial capillaries (van den Berg et al., 2003).

A direct *in vivo* measurement of the SGL thickness with the dye-exclusion technique was first developed by Vink and Duling (Vink and Duling, 1996). Using a 70 kD FITC-dextran plasma tracer, which they showed was sterically excluded by the SGL, they were able to provide the first estimate of the *in vivo* thickness of the SGL in capillaries of hamster cremaster-muscle to be ~0.4–0.5 μm, which is ~15–20% of the radius of the smallest capillaries in the microcirculation. Most recently, the SGL thickness was also estimated as ~0.5 μm in rat mesenteric post-capillary venules by FITC-dextran labeling with intravital microscopy (Gao and Lipowsky, 2010). This estimate of the *in vivo* thickness of the SGL is four to five times greater than previous estimates derived from EM studies. This discrepancy was a catalyst for much of the work that has followed on the estimation of SGL thickness and its function as a barrier in cellular interactions. Using high-resolution, near-wall, intravital fluorescent microparticle image velocimetry (μ-PIV) to examine the velocity profile near the vessel wall in post-capillary venules of the mouse cremaster muscle, Long et al. and Smith et al. (Long et al., 2004; Smith et al., 2003) produced estimates of glycocalyx thickness of order 0.5 μm.

The poor spatial resolution of an intravital optical microscope limits the accurate measurement of the SGL thickness (Pries et al., 2000). New imaging methods have thus been developed by employing laser scanning confocal microscopy and multi-photon microscopy, and fluorescently tagged antibodies to heparan sulfate or hyaluronan binding protein, or wheat germ agglutinin to label major components of the SGL. Application of these new methods has revealed a much thicker SGL in large blood vessels: 4.3–4.5 μm in the mouse common carotid artery (Megens et al., 2007), 2.2 μm in the mouse internal carotid artery (van den Berg et al., 2009) and 2.5 μm in the external carotid artery (Reitsma et al., 2011). Most recently, cryo-EM, that avoids the dehydration artifacts of conventional EM, has revealed a SGL layer thickness of order 10 μm on cultured EC *in vitro* (Ebong et al., 2011).

Although laser scanning confocal microscopy has been used to observe the SGL in large blood vessels, it has not been used to quantify the SGL in microvessels, largely due to difficulties in *in vivo* sample preparation and immunostaining of the SGL. Therefore, the objective of our study was to determine the SGL thickness systemically from aorta to microvessels in both rats and mice. To quantify the SGL thickness on the microvessels of rat mesentery and mouse cremaster muscle *in situ*, we applied a single vessel cannulation and perfusion technique to directly inject FITC-anti-heparan sulfate into a group of microvessels for immuno-labeling the SGL on the vessel wall. We also used anti-heparan sulfate for immuno-labeling the SGL on rat and mouse aortas *ex vivo*. After the SGL labeling, we used high sensitivity and resolution confocal microscopy to determine the glycocalyx thickness in these vessels. Our study provides a new approach for *in situ*/*in vivo* measurement of the SGL thickness in blood vessels of various sizes from less than 10 μm to more than 2 mm diameter.

Materials and methods

Solutions and reagents

Mammalian Ringer solution was used for all dissections and perfusates. Its composition was (in mM) 132 NaCl, 4.6 KCl, 1.2 $MgSO_4$, 2.0 $CaCl_2$, 5.0 $NaHCO_3$, 5.5 glucose, and 20 HEPES. All the materials used in making the Ringer solutions were purchased from Sigma-Aldrich (St. Louis, MO). The pH value was maintained between 7.4 and 7.45 by adjusting the ratio of HEPES acid to base. All perfusates also contained 10 mg/mL bovine serum albumin (BSA, Sigma-Aldrich, St. Louis, MO), called 1% BSA Ringer solution. Phosphate buffered saline (PBS) was from Mediatech Inc (Manassas, VA). 4', 6-diamidino-2-phenylindole (DAPI) was from Invitrogen (Carlsbad, CA). FITC conjugated mouse anti-human heparan sulfate (Anti-HS, 10e4 epitope) was purchased from United States Biological (Swampscott, MA). It was diluted to 1:50 (20 μg/mL) in 1% BSA Ringer solution for labeling heparan sulfate on the microvascular endothelial surface glycocalyx. For labeling aortic endothelial surface glycocalyx, the primary mouse anti- heparan sulfate antibody (1:200) was purchased from Millipore (Billerica, MA), and the secondary FITC-tagged goat anti-mouse IgG (1:200) was from Santa Cruz (Santa Cruz, CA). Heparinase III (15 mU/ml) was from Sigma-Aldrich (St. Louis, MO). FITC-labeled BSA (MW ~66KD, Sigma-Aldrich, St. Louis, MO) was dissolved at 0.75 mg/mL in 1% BSA solution. Tetramethyl rhodamine isothiocyanate (TRITC)-dextran (MW ~155KD, Sigma-Aldrich, St. Louis, MO) 0.25 mg/mL was dissolved in 1% BSA solution. All the solutions were made fresh on the day of use to avoid binding to the serum albumin.

In aorta labeling experiments, triton solution consisted of 0.5% triton x-100 (Sigma-Aldrich, St. Louis, MO), 5% goat serum (Invitrogen, Eugene, OR), 10 mg/mL BSA, and 1 mg/mL saponin (Sigma-Aldrich, St. Louis, MO). This combined solution was used to permeabilize tissues. Then the PBS with 10 mg/mL BSA and 1 mg/mL saponin was used for blocking during antibody staining.

Animal preparation

All experiments were performed on female Sprague–Dawley rats (250–300 g, age 3–4 months), supplied by Hilltop Laboratory Animals (Scottdale, PA), or male C57Bl/6 J mice (Black 6 mice, 12–16 weeks), supplied by Jackson Laboratory (Bar Harbor, ME). All animal care and preparation procedures were approved by the Animal Care and Use Committee at the City College of the City University of New York. Rats were anesthetized with pentobarbital sodium given subcutaneously at the initial dosage of 65 mg/kg followed by an additional 3 mg/dose given as needed. Mice were anesthetized with 2% chloralose and 10% urethane in PBS at the initial dosage 7 μl/kg and an additional 30 μl/dose when needed. The methods used to prepare rat mesenteries and mouse cremaster muscles, perfusion solutions and micropipettes for microperfusion experiments have been described in detail elsewhere (Fu and Shen, 2004; Hidalgo et al., 2007; Shen et al., 2010).

Briefly, for microvessel perfusion and labeling, after a rat was anesthetized, a mid-line surgical incision was made in the abdominal wall. Then the rat was transferred to a tray and kept warm at 37 °C on a heating pad and monitored by a thermometer. The mesentery was carefully taken out from the abdominal cavity and arranged on a glass coverslip to maintain circulation to the intestine and mesentery. Similarly, after a mouse was anesthetized, transferred to a tray and kept warm at 37 °C on a heating pad, its cremaster muscle was carefully exteriorized, opened with cautery, spread and pinned out over a quartz pillar (1 cm in diameter, Heræus-Amersil, Fairfield, NJ) to maintain the circulation. The exposed tissues were continuously superfused in mammalian Ringer's solution at 35 °C-37 °C by a dripper, which was regulated by a controlled water bath and monitored regularly by a thermometer probe. For the microvessels in the cremaster muscle of the adult mouse, we did not see a significant change in the vessel diameter under superfusate of 34.5 °C, 37 °C and 4 °C ($p > 0.2$, data not shown). The vasoconstriction in the small arterioles observed by Hogan et al. (1982) was in the cremaster muscle of the young Wistar rat. The difference in the thermoregulatory mechanism may be due to different species and different ages.

For aorta labeling, after anesthesia, the left femoral vein was located and cannulated by using PE50 polyethylene tubing attached to two syringes, one containing excess sodium pentobarbital and the other containing 0.3 ml of heparin (5000USP unit/ml). The trachea was intubated and mechanically ventilated. The animal was then perfused through the femoral vein with the heparin, immediately followed by

an overdose of sodium pentobarbital through the same vein to stop the heart. The mid-line surgical incision was made from the abdominal wall to thoracic wall. The heart and aorta were exposed after cutting off the ribs. Then 3 mL 2% paraformaldehyde in PBS was injected through the left ventricle using a 5 mL syringe with a 27 G needle. Meanwhile the downstream of the aorta was cut open to remove the blood. After the blood was completely washed away, the thoracic aorta was removed and placed in 2% paraformaldehyde solution.

Immunostaining microvessel glycocalyx

An artery (25–35 μm diameter) supplying the rat mesentery or mouse cremaster muscle was carefully chosen to connect only microvessels in a region of interest, which contained 3–7 arterioles, 5–8 capillaries and 3–8 post-capillary venules. Then this artery was cannulated with a glass theta micropipette with two lumens (see Fig. 1). The making of the theta pipette was described in Fu et al. (Fu et al., 2005; Fu and Shen, 2004). We had tried the FITC-anti-HS immunolabeling of the SGL under superfusate of 35°–37 °C and the room temperature and failed to label the SGL until we used superfusate of 4 °C. The upper surface of the tissue was continuously superfused by a dripper with mammalian Ringer solution at ~4 °C, which was regulated by a controlled water bath with ice and monitored by a thermometer probe. Microvessels were first perfused for 15 min with a blocking solution of 5% goat serum containing 1% BSA Ringer through one lumen of the theta micropipette cannulating the artery by a driving pressure from a water manometer. Then the perfusion was switched to another lumen of the pipette to inject FITC-conjugated anti-heparan sulfate (HS) in 1% BSA Ringer (20 μg/mL) into the microvessels for ~2.5 h. After 15 min perfusion of the first perfusate to wash away the free dye, the vessels were fixed by superfusing the tissue with ice-cold 1% paraformaldehyde for 3–5 min. The animal was sacrificed by anesthetic overdosing. The vessels were perfused until no blood circulation was observed in the tissue and the cannulating micropipette was pulled out of the artery. The tissue (~1 cm × 1 cm) surrounding the vessels was then dissected, rinsed with ice cold PBS, and mounted on a glass coverslip. A secured-seal spacer (Invitrogen, Eugene, OR) was used to surround the tissue and to make a well about 120 μm (or 240 μm for mouse cremaster muscle) deep between two coverslips to retain the three-dimensional structure of the vessels.

To test whether or not the anti-HS stain spanned the entire thickness of the SGL, we also used TRITC-dextran (MW ~ 155kD) and FITC-BSA (MW ~ 66kD) to label the SGL at the microvessel wall. Dextran 155kD has a similar molecular weight as the anti-HS (~180kD), which takes a similar amount of time to transport into the entire SGL on the microvessel wall. The protocol for labeling the SGL by TRITC-dextran was the same as that by FITC-anti-HS while there was a difference for labeling by FITC-BSA. After perfusing FITC-BSA via the theta micropipette cannulating the artery for only 10–15 min instead of 2.5 h, the vessels were fixed by superfusing the tissue with ice-cold 1% paraformaldehyde for 3-5 min, then the vessels were perfused with the solution without dye to wash away the free FITC-BSA for 2–3 min before the animal was sacrificed.

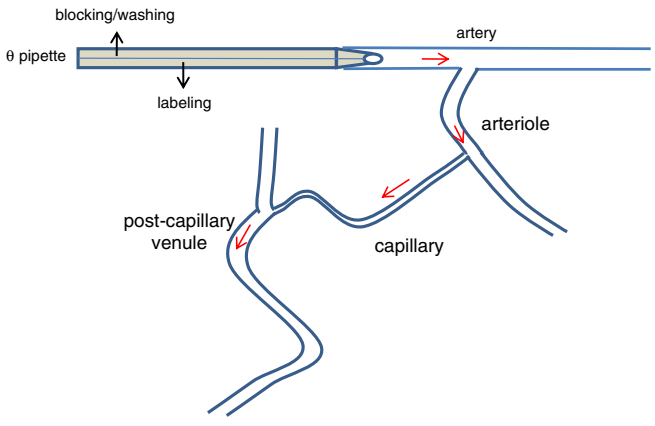

Fig. 1. Schematic showing the single vessel cannulation and perfusion for directly injecting FITC-anti-HS into a group of microvessels via a theta (θ) micropipette cannulating an artery. The blocking solution was first perfused into the microvessels through one lumen of the θ micropipette. Then the perfusion was switched to another lumen to perfuse FITC-anti-HS for immunolabeling the SGL in the microvessels. After labeling, the perfusion was back to the first solution to wash away the free FITC-anti-HS.

Immunostaining aorta glycocalyx

For aorta labeling, connective tissue was first removed from the aorta and the aorta was cut into ~1 cm long rings. After washing with the PBS, the aortic rings were permeabilized for 1 h with triton solution and blocked for 30 min with 1% BSA saponin solution. Then the aorta segments were incubated with mouse anti-heparan sulfate antibody overnight. After a brief wash with PBS, the specimens were blocked for 30 min and incubated with the FITC-labeled goat anti-mouse IgG for 2 h. To determine the endothelial surface at the aortic wall, we also labeled the endothelial cells using DAPI for 10 min. After PBS washing, a ring segment was cut open and the flat segment was placed between two coverslips for imaging by a confocal microscope. To determine the luminal diameter of the aorta, the total length of the cut open segment was measured by a ruler and the diameter was calculated as the total length divided by π.

Confocal microscopy

All samples were examined using 12-bit laser scanning confocal microscopy (LSCM, Zeiss LSM 510 Confocal Microscope System) with a 40X/NA1.3 objective lens. Excitation/Emission wavelength (nm) = 490/525 for FITC, 350/470 for DAPI and 557/576 for TRITC. Images were collected either from the top (near lens) to the bottom or from the bottom to the top (z-direction) for each sample, forming a stack of images along the z-direction. The thickness of each image was 0.2–0.3 μm for a microvessel sample and 0.17 μm for an aorta segment. For an image of 1024 × 1024 pixels, it typically scanned a ~140 μm × 140 μm area of a tissue segment containing a microvessel, resulting in a resolution of ~0.14 μm/pixel; it scanned a ~210 μm × 210 μm area of an aortic segment, resulting in a resolution of ~0.2 μm/pixel.

Image analysis

The image stacks were analyzed with the public domain National Institutes of Health IMAGE J program. Stacks were reconstructed as a 3-D view showing the fluorescence-labeled surface glycocalyx layer (SGL). The stacks were re-sliced into 1 μm thick rings (cross-sections) along the vessel axis. For microvessels of length 80–140 μm, 5–10 cross-sectional slices were analyzed for the SGL thickness. For each slice, 4 lines were drawn across the cross-section (Fig. 2A) and the fluorescence intensity was plotted for each line. The SGL thickness was defined as the distance between two points with half-maximum fluorescence intensity along the line near the wall (green bars in Fig. 2B). Eight thicknesses were averaged for each slice, and the thicknesses for 5–10 slices along the vessel axis were averaged as the SGL thickness for each vessel. For aortic SGL thickness, 4 slices of thickness 1 μm were chosen along the cross-section of an aortic segment of area ~210 μm × 210 μm. Seven lines were drawn along each slice (Fig. 2C). The SGL thickness was defined as the distance between two points with half-maximum fluorescence intensity along the line (green bar in Fig. 2D). Seven thicknesses were averaged for each slice, and the thicknesses for 4 slices were averaged as the SGL thickness for each aorta. To determine the glycocalyx distribution along the microvessel wall, the fluorescence intensity was

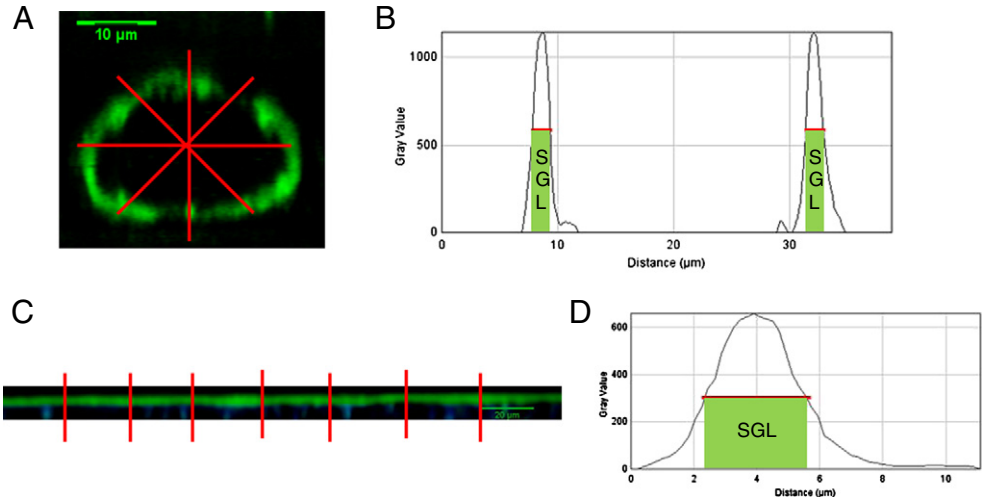

Fig. 2. Schematic for quantification of the surface glycocalyx layer (SGL). For a microvessel, 4 lines were drawn at its cross-section (A). The thickness of the SGL was determined as the distance between two points with the half-maximum fluorescence intensity along the line near the wall, the green shaded regions in (B). The SGL thickness for that cross-section of a microvessel is the average of 8 thicknesses measured along the circumference. The SGL thickness for the microvessel is the average of the thicknesses from 5 to 10 cross-sections along the vessel axis. For an aorta, 7 lines were drawn along a cross-section (C). The thickness of the SGL was determined as the distance between two points with the half-maximum fluorescence intensity along the line, the green shaded region in (D). The SGL thickness for that cross-section of an aorta is the average of 7 thicknesses measured along the cross-section. The SGL thickness of the aorta is the average of the thicknesses from 4 cross-sections at the aorta.

integrated along the wall using the commercial software Matlab (Mathworks, Natick, MA).

Statistics

All data were presented as the mean ± SD, while "n" indicates the number of vessels. Mann–Whitney's U test was applied to test statistical significance between two independent groups. Significance was assumed for probability levels $p<0.05$. The statistical analysis was performed using Sigma Plot 11.2 from Systat Software Inc. (San Jose, CA).

Results

FITC-anti-HS labeled SGL on the microvessels of rat mesenteries and mouse cremaster muscles

Fig. 3A shows the mid-plane view of the SGL labeled with FITC-anti-heparan sulfate (HS) (green) along a rat mesenteric capillary. The 3D re-construction of the SGL is shown in Fig. 3B. Fig. 3C demonstrates the cross-sectional view of 10 slices of thickness 1 μm evenly cut along the segment in the middle of the capillary, 1/4 vessel length from both ends. Overall, for rat mesenteric capillaries of diameter 9.0 ± 0.7 μm (from 8.4 to 9.8 μm), the SGL thickness is 0.9 ± 0.1 μm (from 0.8 to 1.0 μm) (n = 3). For rat mesenteric post-capillary venules of diameter 24.2 ± 9.2 μm (from 13.2 to 48.7 μm), the SGL thickness is 1.2 ± 0.3 μm (from 0.8 to 1.6 μm) (n = 15). Fig. 3D shows the comparison of the SGL thickness of the post capillary venules and the capillaries of rat mesentery. There is no significant difference in the SGL thickness between the capillaries and post-capillary venules ($p=0.13$). Surprisingly, there was no heparan sulfate SGL observed on the rat mesenteric arterioles of diameter 21.6 ± 9.0 μm (from 11.1 to 32.3 μm) (n = 15).

Since it was very hard to find microvessels in the mouse mesentery, we observed the SGL in the microvessels of mouse cremaster muscles. Fig. 4A shows the mid-plane view of the SGL labeled with FITC-anti-HS (green) along a post-capillary venule in the mouse cremaster muscle. The 3D re-construction of the SGL is shown in Fig. 4B. Fig. 4C demonstrates the cross-sectional view of 10 slices of thickness 1 μm evenly cut along the entire vessel. Overall, for mouse cremaster muscle capillaries of diameter 9.1 ± 0.7 μm (from 8.6 to 9.8 μm), the SGL thickness is 1.5 ± 0.2 μm (from 1.3 to 1.6 μm) (n = 3). For mouse cremaster muscle post-capillary venules of diameter 17.1 ± 4.7 μm (from 13.0 to 26.0 μm), the SGL thickness is 1.5 ± 0.1 μm (from 1.3 to 1.8 μm) (n = 13). Fig. 4D provides a comparison of the SGL thickness on post capillary venules and capillaries of the mouse cremaster muscle. As in the rat mesentery, there is no difference in the SGL thickness between post-capillary venules and capillaries in the mouse cremaster muscle ($p=0.69$), and there was no heparan sulfate SGL observed in the arterioles of diameter 23.9 ± 4.8 μm (from 13.5 to 29.8 μm) (n = 13).

FITC-anti-HS labeled SGL on the aortas of rats and mice

In addition to the SGL on the microvessels of rats and mice, we quantified the SGL on their aortas. Fig. 5 shows a confocal image for FITC-anti-HS (green) on the surface of a cut open mouse aorta. Fig. 5A is the 3D view of a 210 × 210 μm area of the aorta and Fig. 5B is the cross-sectional view. To determine the orientation of the endothelial cell surface, we used DAPI to label the endothelial cell nuclei (blue). The SGL was always above the blue region. Its thickness was determined using the method described in Fig. 2C, D. For the rat aorta of diameter 2.0 ± 0.01 mm (from 2.0 to 2.3 mm), the SGL thickness is 2.5 ± 0.1 μm (from 2.4 to 2.6 μm) (n = 3). For the mouse aorta of diameter 0.67 ± 0.07 mm (from 0.65 to 0.69 mm), the SGL thickness is 2.1 ± 0.2 μm (from 1.9 to 2.3 μm) (n = 3). Fig. 5C demonstrates the distribution of the integrated intensity of FITC-anti-HS along a mouse aorta (Fig. 5B). Fig. 5D shows that there is no significant difference in the SGL thickness between rat and mouse aortas ($p=0.43$). The distribution of the FITC-anti-HS along the rat aorta is also similar to that along the mouse aorta.

Distribution of the SGL along the microvessels of rat mesentery and mouse cremaster muscles

To test whether or not the SGL is evenly distributed along the microvessels of rat mesentery and mouse cremaster muscles, we plotted the integrated intensity of FITC-anti-HS along the microvessel wall in the mid-plane section of thickness 0.2–0.3 μm (Figs. 3A, 4A). The integrated intensity was defined as the integration of the fluorescence intensity along the radial direction over the region where there was SGL labeling at one wall of the vessel (Fig. 2B). Then the integrated intensity was normalized by the maximum integrated

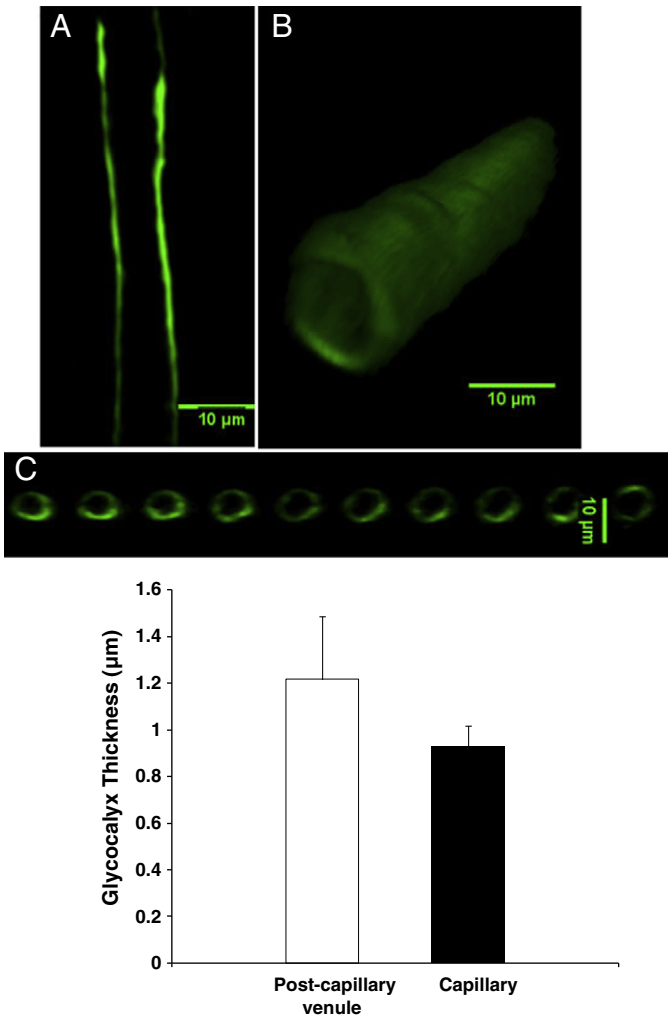

Fig. 3. Confocal images of the FITC-anti-HS labeled SGL in a rat mesenteric capillary. Image at the mid-plane of the capillary (A), 3D reconstruction (B) and cross-sectional views along the capillary axis (C). (D) shows the comparison of the thickness of the SGL on the post-capillary venules (n = 15) with that on the capillaries (n = 3) of rat mesentery. There was no SGL observed in arterioles (n = 15).

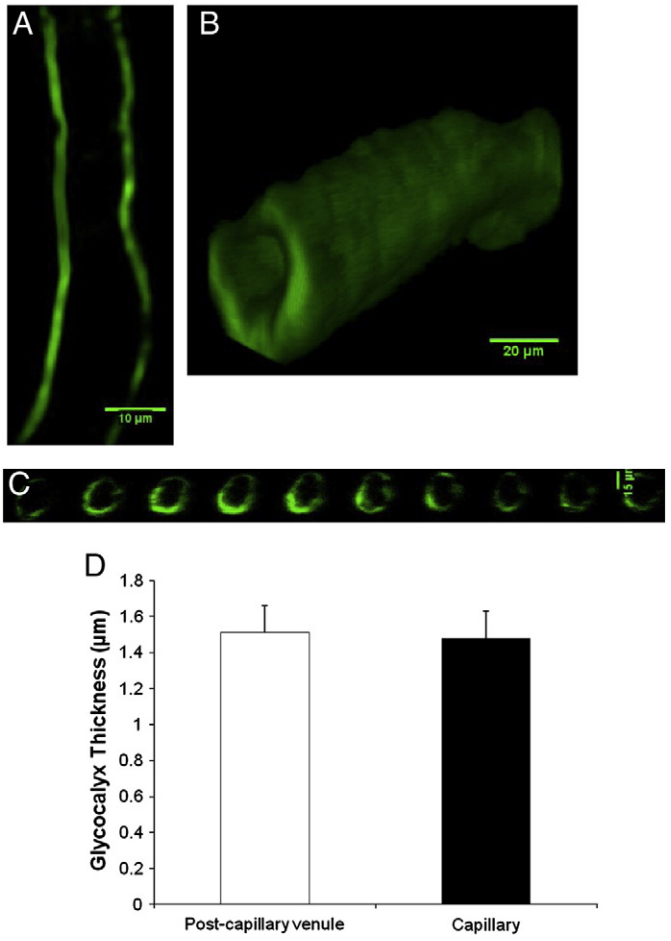

Fig. 4. Confocal images of the FITC-anti-HS labeled SGL in a post-capillary venule in a mouse cremaster muscle. Image at the middle-plane of the post-capillary venule (A), 3D reconstruction (B) and cross-sectional views along the post-capillary venule axis (C). (D) shows the comparison of the thickness of the SGL on the post-capillary venules (n = 13) with that on the capillaries (n = 3) of mouse cremaster muscle. There was no SGL observed in arterioles (n = 13).

intensity at that wall of the vessel. Fig. 6A shows the SGL labeling in the mid-plane along one wall of a post-capillary venule with length ~120 μm in the mouse cremaster muscle. Fig. 6B shows the normalized integrated intensity distribution along the same wall. The label "Y" (blue) indicates a wall segment with significant SGL while the label "N" (red) indicates a segment with undetectable or insignificant SGL. The "Y" was defined as a segment with an averaged normalized intensity of at least 0.5 while the "N" was defined as a segment with an averaged normalized intensity less than 0.2. The averaged normalized intensity over a segment of length L is $\frac{\int_0^L I(x)dx}{L}$, where x is the axial coordinate and I(x) is the normalized integrated intensity at location x (Fig. 6B). The SGL thickness reported for each vessel in this study (Figs. 3–5) was the average of the "Y" segments where there was significant SGL.

According to the above criteria, the average length of the "Y" segments in the post-capillary venules of rat mesenteries is 30.7 ± 20.5 μm and that of the "N" segments is 30.5 ± 12.0 μm (n = 15). The total "Y" segments account for 44.7 ± 13.6% of the total length (two sides) of the vessels while the total "N" segments account for 55.3 ± 13.4% (n = 15). The difference in the percentage between the "Y" and "N" segments in rat mesenteric post-capillary venules is nearly significant (p = 0.051). Similarly, the average length of the "Y" segments and that of the "N" segments in rat mesenteric capillaries is 27.1 ± 10.3 μm and 28.1 ± 15.1 μm (n = 3), respectively. No significant difference was found in the percentage between the "Y" (39.2 ± 19.1%) and "N" segments (60.8 ± 19.1%) (p = 0.24).

Following the same definition, the average length of the "Y" segments in the post-capillary venules of mouse cremaster muscles is 20.3 ± 8.8 μm and that of "N" segments is 13.5 ± 6.0 μm (n = 13). There is no significant difference in the percentage between the "Y" (54.8 ± 12.6%) and the "N" segments (44.7 ± 12.8%) (p = 0.08). For capillaries in mouse cremaster muscles, the average length of the "Y" segments is 63.9 ± 17.2 μm and that of the "N" segments 33.3 ± 21.4 μm (n = 3). No significant difference was found in the percentage between the "Y" (56.8 ± 9.1%) and the "N" segments (43.2 ± 9.1%) (p = 0.14).

In Fig. 6C, we compared the percentages of the "Y" and "N" segments in the microvessels of the rat mesentery and mouse cremaster muscles. Although there is a slightly lower percentage of the segments covered with the significant SGL in the rat mesenteric microvessels than in the mouse cremaster muscle microvessels, the difference is not significant (p > 0.05). Interestingly, compared to only about half of the walls covered with the SGL in the microvessels, almost 100% of the surface was covered with the SGL in both rat and mouse aortas (Fig. 5C).

Discussion

It is well established that the endothelial surface glycocalyx layer (SGL) contains a wide variety of membrane-bound carbohydrate-

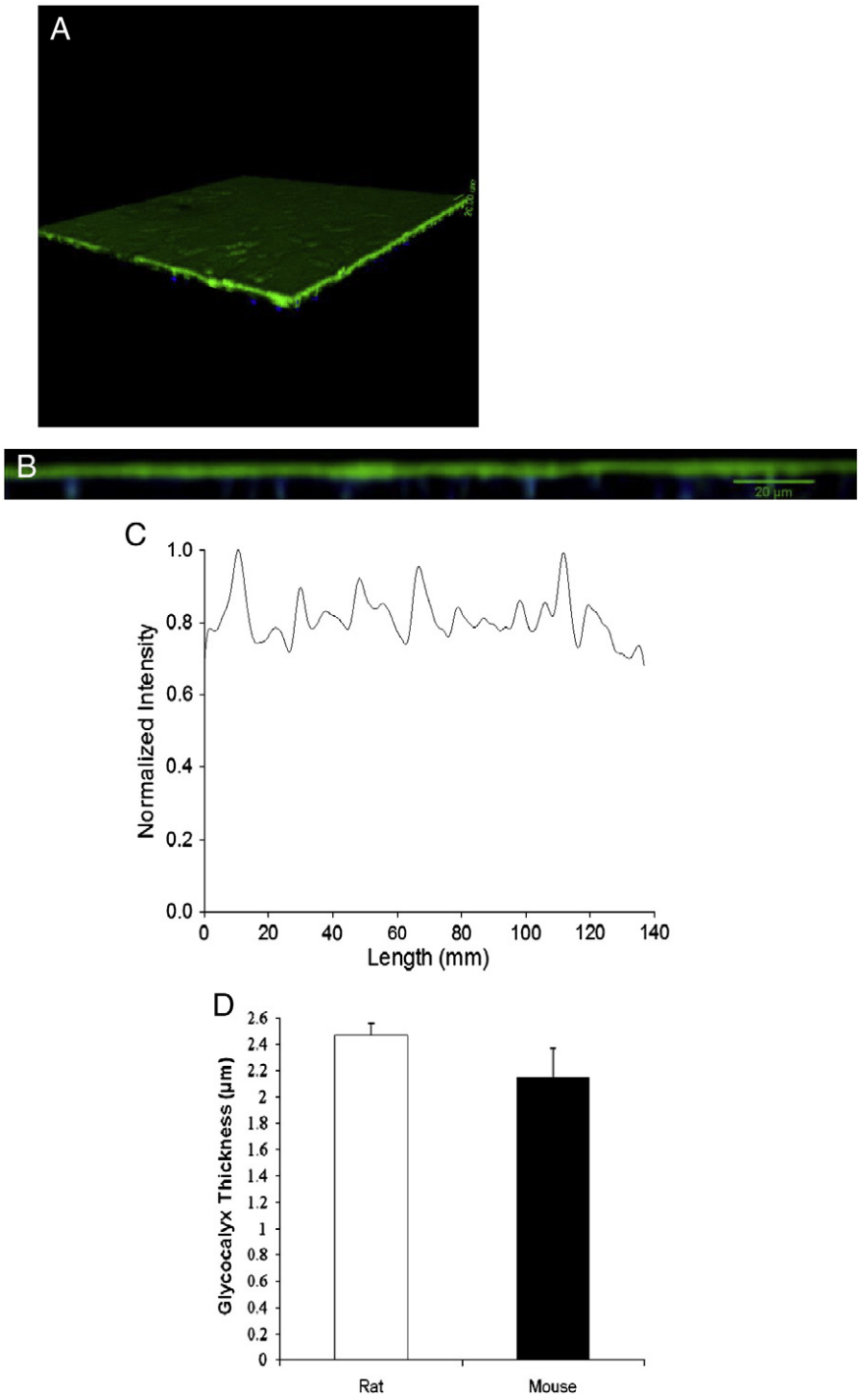

Fig. 5. Confocal images of the FITC-anti-HS labeled SGL (green) in a mouse aorta. The blue indicates the endothelial cell nuclei labeled with DAPI. 3D reconstruction (A) and a cross-sectional view (B). (C) Normalized fluorescence intensity of FITC-anti-HS along the wall of the same aorta in (B). (D) shows the comparison of the thickness of the SGL on the rat aortas (n = 3) with the mouse aortas (n = 3).

rich macromolecules (Schnitzer et al., 1988), glycosaminoglycans (GAGs), which include heparan sulfate (HS), chondroitin sulfate, dermatan sulfate, keratin sulfate and hyaluronic acid or hyaluronan (HA) (Oohira et al., 1983; Reitsma et al., 2007). HS is one of the most abundant, which is ~50-90% of the total GAGs (Oohira et al., 1983; Tarbell and Pahakis, 2006). Therefore by measuring the layer of HS specifically bound with fluorescently-tagged anti-HS, we can estimate the SGL thickness. Following this approach, Stevens et al. (2007) found that the HS and HA layers on fixed lung microvascular endothelial monolayers are 2-3 μm thick (Stevens et al., 2007). In our *in vivo* immunostaining study, we found that the thickness of the HS layer ("Y" segments as described above) is 1.2 ± 0.3 and 0.9 ± 0.1 μm, respectively, in rat mesenteric post-capillary venules and capillaries while it is 1.5 ± 0.2 μm in mouse cremaster muscle post-capillary venules and capillaries. We also found that there is no significant difference in the HS layer thickness in different types of microvessels and in the microvessels of rats and mice. The SGL thickness of order ~1 μm observed in these microvessels using immunolabeling and high resolution confocal microscopy in the current study is 2–3 times that of microvessel SGL thickness estimated by a variety of *in vivo* intravital microscopy techniques with much lower spatial resolution (Gao and Lipowsky, 2010; Smith et al., 2003; Vink et al., 2000; Vink and

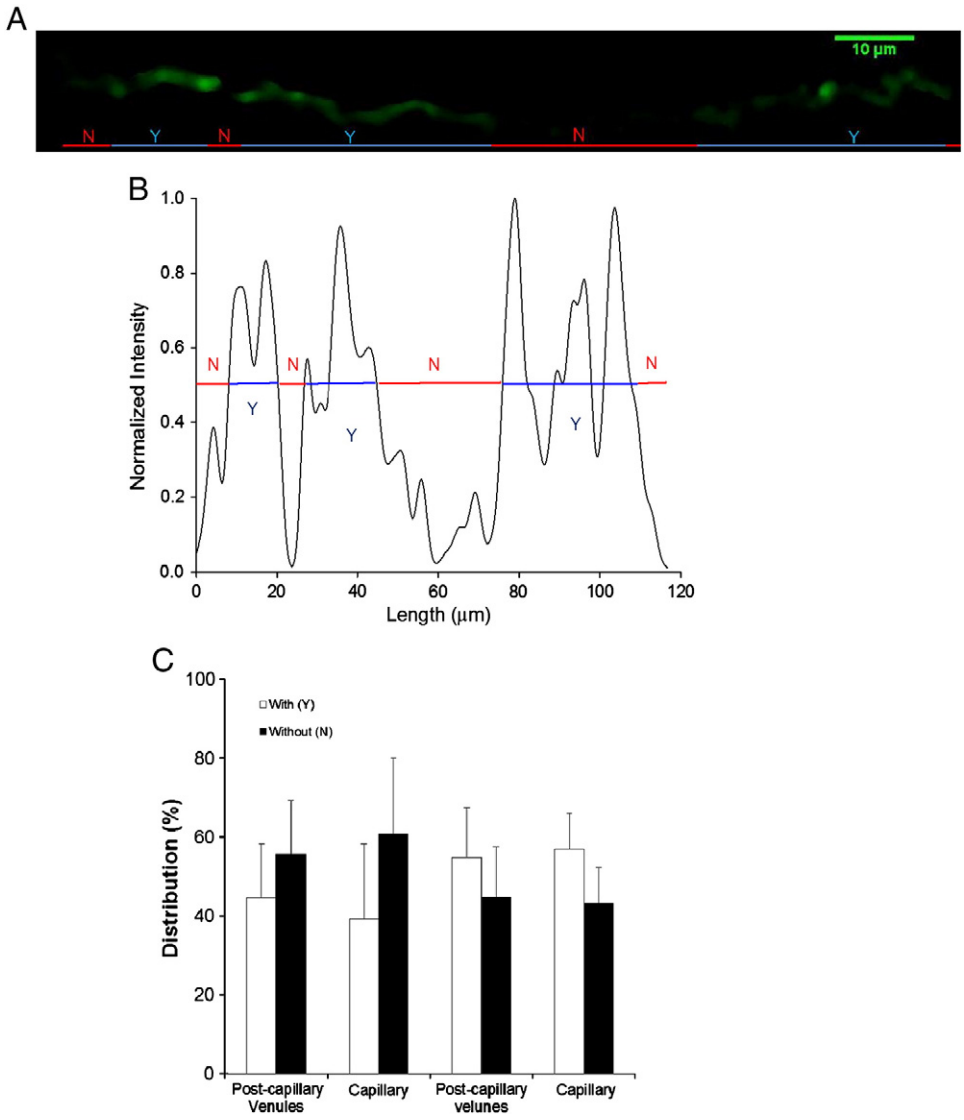

Fig. 6. The surface glycocalyx distribution along the wall of microvessels. Image at the mid-plane of a representative post-capillary venule at a mouse cremaster muscle (A). Normalized fluorescence intensity of FITC-anti-HS along the wall of the same vessel (B). The segments with the same numerical labels in (A) and (B) are identical. Label "Y" indicates the wall segments with the significant SGL while label "N" indicates those with undetectable or insignificant SGL. (C) shows the percentage of the "Y" and "N" segments in the post-capillary venules (n = 15) and capillaries (n = 3) of rat mesenteries, and in the post-capillary venules (n = 13) and capillaries (n = 3) of mouse cremaster muscles.

Duling, 1996). This SGL thickness is also about 10 times that measured by EM in similar types of microvessels. The much thinner SGL thickness measured by EM may be due to the collapse of the SGL under dehydration during chemical fixation (Pries et al., 2000; Squire et al., 2001).

Since anti-HS has a molecular weight of ~180 kD, it may not bind to the HS in the entire SGL due to steric resistance of the SGL's fiber matrix structure. This may cause an underestimation of the SGL thickness. Although we locally perfused anti-HS for 2.5 h, which is more than sufficient for a molecule like anti-HS to diffuse through a distance of several microns in aqueous solution, we tested whether or not the entire SGL was labeled with the anti-HS, by perfusing a smaller sized FITC-BSA (~66kD) and a similar sized TRITC-Dextran (155kD). Fig. 7A shows the confocal images for the mid-plane view of the SGL labeled with FITC-anti-HS, FITC-BSA and TRITC-Dextran155kD in rat mesenteric post-capillary venules. The respective SGL thickness obtained by these 3 labelings is 1.2 ± 0.3 μm, 1.5 ± 0.1 μm and 1.4 ± 0.1 μm ($n = 5$) (Fig. 7B). That there is no significant difference in the SGL thickness labeled by anti-HS, BSA and Dextran155kD ($p > 0.09$) indicates that anti-HS has penetrated and labeled the entire SGL by applying our *in situ* single vessel perfusion immunolabeling method.

In the SGL fluorescence labeling, we identified the edge of the microvessel endothelial cells (EC) by using our 20×/NA0.75 imaging system under bright field and the fluorescent light (Gao and Lipowsky, 2010) to ensure that the fluorescence labeling was at the luminal side of the EC. We also performed FITC-ZO-1 and TRITC-BSA co-labeling for the EC tight junctions and the SGL to locate the EC in some vessels and confirmed that the SGL was on the luminal EC surface (data not shown). The thickness of the TRITC-BSA labeled SGL in the co-labeling preparation was ~0.9 μm and had no significant difference from that labeled with FITC-anti-HS. In the future, we will use transgenic rats/mice with GFP expressed EC to precisely determine the EC boundary.

Using a medium resolution confocal microscope (0.37 μm/pixel), van Haaren et al. (van Haaren et al., 2003) estimated a ~3 μm thick SGL in isolated rat mesenteric arteries (diameter ~150 μm) by observing the exclusion zone of FITC-dextran of high molecular weight. Applying intravital fluorescence micro-particle image velocimetry, Savery and Damiano (Savery and Damiano, 2008) estimated that the SGL thickness is ~0.38 μm in mouse cremaster muscle arterioles (diameter 20-70 μm), which is 0.13 μm thinner than that in venules having a similar diameter range. Unexpectedly, using our *in situ* single

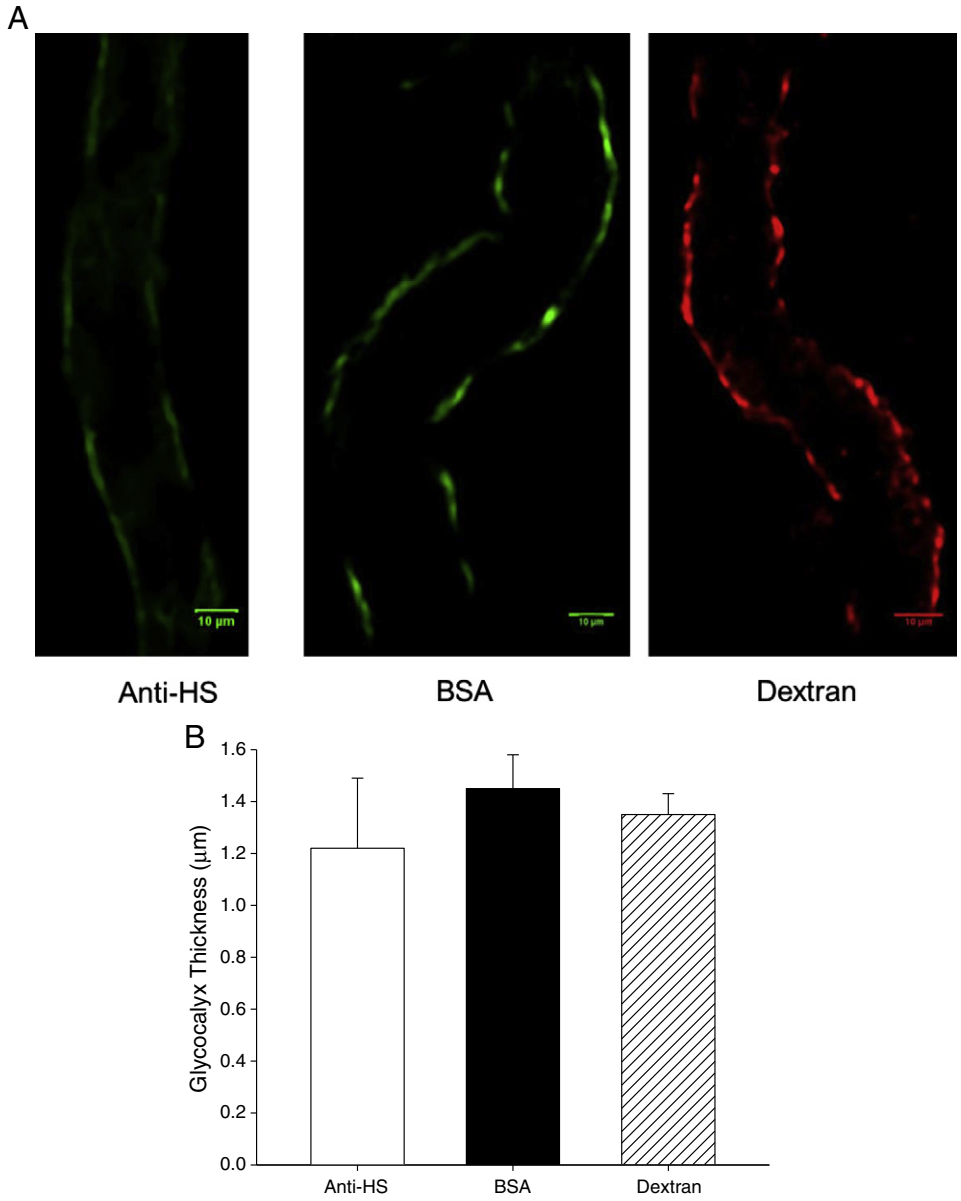

Fig. 7. Confocal images of the SGL labeled by FITC-anti-HS, FITC-BSA and TRITC-Dextran 155kD in post-capillary venules of rat mesentery (A). Comparison of the SGL thickness determined from FITC-anti-HS labeling (n = 15), FITC-BSA labeling (n = 5) and TRITC-dextran labeling (n = 5) in the post-capillary venules of rat mesentery.

vessel perfusion immunolabeling method, we did not observe any glycocalyx in arterioles of either the rat mesentery (diameter 21.6 ± 9.0 μm, ranging from 11.1 to 32.3 μm) or mouse cremaster muscle (diameter 23.9 ± 4.8 μm, ranging from 13.5 to 29.8 μm). To rule out the possibility that HS is not rich enough or absent in arterioles, in addition to FITC-anti-HS, we used FITC-BSA, TRITC-Dextran 155kD and Dextran 70kD to label the SGL and failed to see the labeling of arterioles. To test another possibility that a higher perfusion velocity in an arteriole may wash away the labeling, we cannulated a single arteriole and maintained a perfusion velocity near zero (<100 μm/s). No SGL labeling was observed. To further investigate the reason for the absence of SGL labeling in arterioles, we compared the conditions of our single vessel perfusion immunolabeling method with others in the literature. One distinctive difference is that circulating blood was present in all other intravital microscopy methods but not in our method. Using a method that was described in Gao and Lipowsky (Gao and Lipowsky, 2010), we observed a thin FITC-Dextran 70kD layer trapped between the circulating blood cells and the arteriole wall by intravital microscopy with an objective lens of 20X/NA0.75. The thickness of this trapped FITC-Dextran layer was estimated to be ~0.5 μm by using a 5-parameter sigmoidal fitting curve as in (Gao and Lipowsky, 2010).

The above discussion presents two discrepancies between the current more specific method and others in the literature. The first discrepancy is that we did not observe SGL labeling at the wall of arterioles but it could be clearly seen at the wall of capillaries and post-capillary venules in the same animal when we washed away the free dye. One explanation is that when there is blood present, the free dye can be trapped in between the blood cells and the vessel wall regardless of the existence of the SGL. The trapped liquid is required for lubrication during RBC movement. The intravital microscopy studies in the literature (Gao and Lipowsky, 2010; Smith et al., 2003; Vink et al., 2000; Vink and Duling, 1996) could not distinguish the trapped free dye and the dye bound by the SGL. By washing away the free dye, our method is able to detect the dye bound by the SGL. To confirm the existence of a SGL on the capillary and post-capillary venule, we pretreated the vessels with 15 mU/ml heparinase III for 1 h, and no SGL was detected in any type of microvessels. The second

discrepancy is that the SGL thickness was estimated as ~0.5 μm at the wall of all types of microvessels when circulating blood was present in the vessel. The SGL thickness of ~0.5 μm is significantly smaller than ~1 μm, which was observed in the present study when circulating blood was absent. A thicker SGL associated with the "build up" of labeling dye was unlikely since we washed away the free dye and did not see a higher dye intensity at the tip of the SGL. A plausible explanation for this difference is that when blood is present, the blood cells apply a normal force on the microvessel wall that can compress the SGL and reduce its unconstrained thickness. Further investigation is required to unravel these discrepancies.

Since our current method cannot determine the SGL thickness without paraformaldehyde fixation, the SGL thickness may be underestimated due to the fact that the paraformaldehyde-preserved SGL is distorted because of aldehyde-induced cross-linking of SGL components and subsequent pulling of the SGL inward toward the cell surface (Ebong et al., 2011).

Few studies have investigated the SGL in the aorta, the largest vessel in the cardiovascular system. By using *ex vivo* immunostaining and high resolution laser scanning confocal microscopy, we observed the SGL thickness in both rat and mouse aortas to be 2.5 ± 0.1 μm and 2.1 ± 0.2 μm, respectively. Compared with other studies using confocal microscopy and two-photon laser scanning microscopy, this SGL thickness in aortas is thinner than in mouse common carotid arteries (~4.3 μm), similar to the internal carotid artery (~2.2 μm) (van den Berg et al., 2009) and the external carotid artery (~2.5 μm) (Reitsma et al., 2011). The SGL was also visualized by EM in vessels ranging from arteries to vena cava in rabbits by fixation with glutaraldehyde containing Alcian blue. The order of increasing SGL thickness was: inferior vena cava ≤ thoracic aorta < aortic arch < carotid artery (Haldenby et al., 1994). Compared with the SGL thickness in mouse carotid arteries (van den Berg et al., 2009), the thinner SGL in thoracic aortas that we observed follows the pattern described in (Haldenby et al., 1994). Using a perfusion-fixed EM to stabilize the SGL, Chappell et al. (2009) observed a ~1 μm thick SGL on human umbilical veins. However the mechanisms that dictate a broad range of SGL thicknesses in the arterial and venule systems are not clear.

The SGL was first visualized by EM, which revealed an irregular, but uniformly distributed layer extending into the microvessel lumen (Gouverneur et al., 2006; Lindner et al., 1998; Squire et al., 2001). Vink and Duling demonstrated that hamster cremaster muscle capillaries (diameter ~5 μm) lined with a uniform SGL *in vivo* by estimating the exclusion zone of the FITC-dextran (Vink and Duling, 1996). All of these previous studies measured the SGL distribution in a vessel segment of length 5 μm or less. In our study, we investigated the SGL distribution over a vessel segment of length ~100 μm for microvessels and ~200 μm for aortas. We found that the SGL was uniformly distributed in rat and mouse aortas but not in the microvessels. Fig. 6 shows that only about half of the microvessel wall is covered with a substantial SGL ("Y" segments). Another half may not be covered or covered with a much thinner SGL. The average length of segments covered with substantial SGL is 20 to 64 μm in different types of microvessels in rats and mice. The shortest length of segments covered with substantial SGL was 10 μm and the longest length was 80 μm over all the microvessels in this study. Our confocal microscopy showed that there is ~1 μm thick SGL on the microvessel wall using the single vessel perfusion method. This thickness is larger than the estimation (~0.5 μm) of others when there was circulating blood in the vessel. So far we cannot tell to what extent the perfusate without the blood would damage the SGL.

Note that the SGL thickness is associated with vessel permeability (Haldenby et al., 1994). The uniformly distributed SGL in aortas implies a relatively constant permeability in the un-diseased aorta while the non-uniformly distributed SGL in microvessels reflects varied permeability along the length of microvessels. The SGL is also a barrier between circulating cells and the ECs forming the microvessel wall. The segments with a thinner SGL in the capillary and post-capillary venule may allow interactions between the circulating cells (white blood cells, platelets and tumor cells) and ECs, resulting in cell adhesion and extravasation (Constantinescu et al., 2003; Haldenby et al., 1994; Vink et al., 2000). The absence of SGL (or much thinner and dilute) in arterioles makes it easier for the circulating cells to make contact with the ECs. But the higher flow velocity in arterioles generates a larger tangential force, which prevents the adhesion of the circulating cells to the ECs (Yan et al., 2010). Additional physiological relevance for the significant SGL in the capillary is that the fiber-matrix like SGL, when compressed by a passing RBC that squeezes out plasma, can provide much higher normal force on the RBC than the plasma alone. This normal force can deform the RBC making it possible to pass through the narrow capillary (Weinbaum et al., 2007; Wu et al., 2004).

Our observation that there is no detectable SGL in arterioles but significant SGL in venules and capillaries is consistent with studies by Williams (1999) and Kim et al. (2005) that observed a fluid shear stress-dependent increase in hydraulic conductivity (Lp) in venules and capillaries, but not arterioles. Shear-dependent increases in Lp are thought to be a consequence of shear-induced increases in nitric oxide production mediated by the endothelial SGL (Tarbell, 2010).

In summary, we have for the first time quantified the SGL thickness in the rat and mouse blood vessels from microvessels to aorta. Compared to EM and intravital microscopy approaches, our method using *in vivo* immunolabeling and laser scanning confocal microscopy overcomes the dehydration artifacts, specifies the SGL component, and improves the spatial resolution of the collected images. However, to further investigate the detailed structure of the SGL and solve the mystery that there was no detectable SGL in arterioles, we will use cryo-EM as described in (Ebong et al., 2011) for viewing the SGL in rat and mouse vessels.

Acknowledgments

This work was supported by NIH/NHLBI 1R01HL094889.

References

Adamson, R.H., Clough, G., 1992. Plasma proteins modify the endothelial cell glycocalyx of frog mesenteric microvessels. J. Physiol. 445, 473–486.
Baldwin, A.L., Winlove, C.P., 1984. Effects of perfusate composition on binding of ruthenium red and gold colloid to glycocalyx of rabbit aortic endothelium. J. Histochem. Cytochem. 32, 259–266.
Becker, B.F., et al., 2010. Endothelial glycocalyx and coronary vascular permeability: the fringe benefit. Basic Res. Cardiol. 105, 687–701.
Chappell, D., et al., 2011. Sevoflurane Reduces Leukocyte and Platelet Adhesion after Ischemia-Reperfusion by Protecting the Endothelial Glycocalyx. Anesthesiology 115, 483–491.
Chappell, D., et al., 2009. The glycocalyx of the human umbilical vein endothelial cell: an impressive structure ex vivo but not in culture. Circ. Res. 104, 1313–1317.
Clough, G., Moffitt, H., 1992. Immunoperoxidase labelling of albumin at the endothelial cell surface of frog mesenteric microvessels. Int. J. Microcirc. Clin. Exp. 11, 345–358.
Constantinescu, A.A., et al., 2003. Endothelial cell glycocalyx modulates immobilization of leukocytes at the endothelial surface. Arterioscler. Thromb. Vasc. Biol. 23, 1541–1547.
Curry, F.R., Adamson, R.H., 2010. Vascular permeability modulation at the cell, microvessel, or whole organ level: towards closing gaps in our knowledge. Cardiovasc. Res. 87, 218–229.
Curry, F.R., Noll, T., 2010. Spotlight on microvascular permeability. Cardiovasc. Res. 87, 195–197.
Ebong, E.E., et al., 2011. Imaging the Endothelial Glycocalyx In Vitro by Rapid Freezing/Freeze Substitution Transmission Electron Microscopy. Arterioscler. Thromb. Vasc. Biol. 31, 1908–1915.
Fu, B.M., et al., 2005. Determination of microvessel permeability and tissue diffusion coefficient of solutes by laser scanning confocal microscopy. J. Biomech. Eng. 127, 270–278.
Fu, B.M., Shen, S., 2004. Acute VEGF effect on solute permeability of mammalian microvessels in vivo. Microvasc. Res. 68, 51–62.
Gao, L., Lipowsky, H.H., 2010. Composition of the endothelial glycocalyx and its relation to its thickness and diffusion of small solutes. Microvasc. Res. 80, 394–401.
Gouverneur, M., et al., 2006. Vasculoprotective properties of the endothelial glycocalyx: effects of fluid shear stress. J. Intern. Med. 259, 393–400.

Haldenby, K.A., et al., 1994. Focal and regional variations in the composition of the glycocalyx of large vessel endothelium. J. Vasc. Res. 31, 2–9.
Hidalgo, A., et al., 2007. Complete identification of E-selectin ligands on neutrophils reveals distinct functions of PSGL-1, ESL-1, and CD44. Immunity 26, 477–489.
Hogan, R.D., et al., 1982. Arteriolar vasoconstriction in rat cremaster muscle induced by local heat stress. Am. J. Physiol. 242 (6), H996–H999.
Kim, M.H., et al., 2005. Regulation of capillary hydraulic conductivity in response to an acute change in shear. Am. J. Physiol. 289, H2126–H2135.
Lindner, J.R., et al., 1998. Albumin microbubble persistence during myocardial contrast echocardiography is associated with microvascular endothelial glycocalyx damage. Circulation 98, 2187–2194.
Long, D.S., et al., 2004. Microviscometry reveals reduced blood viscosity and altered shear rate and shear stress profiles in microvessels after hemodilution. Proc. Natl. Acad. Sci. U. S. A. 101, 10060–10065.
Luft, J.H., 1966. Fine structures of capillary and endocapillary layer as revealed by ruthenium red. Fed. Proc. 25, 1773–1783.
Megens, R.T., et al., 2007. Two-photon microscopy of vital murine elastic and muscular arteries. Combined structural and functional imaging with subcellular resolution. J. Vasc. Res. 44, 87–98.
Mulivor, A.W., Lipowsky, H.H., 2009. Inhibition of glycan shedding and leukocyte-endothelial adhesion in postcapillary venules by suppression of matrixmetalloprotease activity with doxycycline. Microcirculation 16, 657–666.
Oohira, A., et al., 1983. Sulfated proteoglycans synthesized by vascular endothelial cells in culture. J. Biol. Chem. 258, 2014–2021.
Pries, A.R., et al., 2000. The endothelial surface layer. Pflügers Arch. Eur. J. Physiol. 440, 653–666.
Reitsma, S., et al., 2011. Endothelial Glycocalyx Structure in the Intact Carotid Artery: A Two-Photon Laser Scanning Microscopy Study. J. Vasc. Res. 48, 297–306.
Reitsma, S., et al., 2007. The endothelial glycocalyx: composition, functions, and visualization. Pflügers Arch. Eur. J. Physiol. 454, 345–359.
Rostgaard, J., Qvortrup, K., 1997. Electron microscopic demonstrations of filamentous molecular sieve plugs in capillary fenestrae. Microvasc. Res. 53, 1–13.
Savery, M.D., Damiano, E.R., 2008. The endothelial glycocalyx is hydrodynamically relevant in arterioles throughout the cardiac cycle. Biophys. J. 95, 1439–1447.
Schnitzer, J.E., et al., 1988. Albumin interacts specifically with a 60-kDa microvascular endothelial glycoprotein. Proc. Natl. Acad. Sci. U. S. A. 85, 6773–6777.
Shen, S., et al., 2010. Vascular endothelial growth factor enhances cancer cell adhesion to microvascular endothelium in vivo. Exp. Physiol. 95, 369–379.
Sims, D.E., Horne, M.M., 1993. Non-aqueous fixative preserves macromolecules on the endothelial cell surface: an in situ study. Eur. J. Morphol. 31, 251–255.
Smith, M.L., et al., 2003. Near-wall micro-PIV reveals a hydrodynamically relevant endothelial surface layer in venules in vivo. Biophys. J. 85, 637–645.
Squire, J.M., et al., 2001. Quasi-periodic substructure in the microvessel endothelial glycocalyx: a possible explanation for molecular filtering? J. Struct. Biol. 136, 239–255.
Stevens, A.P., et al., 2007. Fluorescence correlation spectroscopy can probe albumin dynamics inside lung endothelial glycocalyx. Am. J. Physiol. Lung Cell. Mol. Physiol. 293, L328–L335.
Tarbell, J.M., 2010. Shear stress and the endothelial transport barrier. Cardiovasc. Res. 87, 320–330.
Tarbell, J.M., Pahakis, M.Y., 2006. Mechanotransduction and the glycocalyx. J. Intern. Med. 259, 339–350.
van den Berg, B.M., et al., 2009. Impaired glycocalyx barrier properties contribute to enhanced intimal low-density lipoprotein accumulation at the carotid artery bifurcation in mice. Pflügers Arch. Eur. J. Physiol. 457, 1199–1206.
van den Berg, B.M., et al., 2003. The endothelial glycocalyx protects against myocardial edema. Circ. Res. 92, 592–594.
van Haaren, P.M., et al., 2003. Localization of the permeability barrier to solutes in isolated arteries by confocal microscopy. Am. J. Physiol. Heart Circ. Physiol. 285, H2848–H2856.
VanTeeffelen, J.W., et al., 2010. Agonist-induced impairment of glycocalyx exclusion properties: contribution to coronary effects of adenosine. Cardiovasc. Res. 87, 311–319.
Vink, H., et al., 2000. Oxidized lipoproteins degrade the endothelial surface layer : implications for platelet-endothelial cell adhesion. Circulation 101, 1500–1502.
Vink, H., Duling, B.R., 1996. Identification of distinct luminal domains for macromolecules, erythrocytes, and leukocytes within mammalian capillaries. Circ. Res. 79, 581–589.
Weinbaum, S., et al., 2007. The structure and function of the endothelial glycocalyx layer. Annu. Rev. Biomed. Eng. 9, 121–167.
Williams, D.A., 1999. Network assessment of capillary hydraulic condoctivity after abrupt changes in fluid shear stress. Microvasc. Res. 57, 107–117.
Wu, Q., et al., 2004. From red cells to snowboarding: a new concept for a train track. Phys. Rev. Lett. 93, 194–501.
Yan, W.W., et al., 2010. Effects of curvature and cell-cell interaction on cell adhesion in microvessels. Biomech. Model. Mechanobiol. 9, 629–640.